

On the behavior of micro-spheres in a hydrogen pellet target

Ö. Nordhage^{a,*}, Z.-K. Li^{b,*}, C.-J. Fridén^c, G. Norman^c, and U. Wiedner^a

^a*Department of Radiation Sciences, Uppsala University, Box 535, SE-751 21 Uppsala, Sweden*

^b*Institute of Modern Physics, the Chinese Academy of Science, Lanzhou, 730000, China*

^c*The Svedberg Laboratory, Uppsala University, Box 533, SE-751 21 Uppsala, Sweden*

Abstract

A pellet target produces micro-spheres of different materials, which are used as an internal target for nuclear and particle physics studies. We will describe the pellet hydrogen behavior by means of fluid dynamics and thermodynamics. In particular one aim is to theoretically understand the cooling effect in order to find an effective method to optimize the working conditions of a pellet target. During the droplet formation the evaporative cooling is best described by a multi-droplet diffusion-controlled model, while in vacuum, the evaporation follows the (revised) Hertz–Knudsen formula. Experimental observations compared with calculations clearly indicated the presence of supercooling, the effect of which is discussed as well.

Key words: Internal target; Hydrogen target; Droplet; Pellet; Evaporative cooling; Supercooling; Nucleation.

PACS: 68.10.Jy, 44.25.+f, 64.70.Dv, 25.75.Dw, 07.20.Mc

1 Introduction

The usage of internal targets in storage-ring accelerators has opened up a new era for the investigations of nucleon-nucleon collisions with high preci-

* Corresponding authors.

Email addresses: orjan.nordhage@tsl.uu.se (Ö. Nordhage), lizhankui@impcas.ac.cn (Z.-K. Li).

sion in hadron physics. The figure of merit for physics experiments is usually the (integrated) luminosity, i.e. the target thickness times the particle beam intensity. For light targets such as hydrogen or deuterium it is quite difficult to achieve the necessary high luminosity with a conventional gas target. The alternative of using frozen micro-spheres, so-called pellets, has been suggested and a prototype pellet-generator was developed by Trostell [1]. A pellet target avoids unnecessary background gas load to the accelerator ring and allows an effective target thickness of a few times 10^{15} atoms/cm² [2,3]. Since the target tubes connected to the accelerator ring are rather narrow, detectors can be placed close to the interaction point in a nearly 4π sr configuration. These particular characteristics of a pellet target have caused worldwide attention, and in the near future pellet target facilities are foreseen in Jülich, Germany, and in Lanzhou, China. Furthermore, this kind of target is considered as one of the main options for the future PANDA experiment [4] at FAIR in Darmstadt, Germany.

Until now there is only one pellet target facility permanently installed and actively operated inside a storage-ring accelerator. It is connected to the WASA (Wide Angle Shower Apparatus) detector at CELSIUS at The Svedberg Laboratory, Uppsala, Sweden. This target has successfully provided hydrogen pellets for experimental data taking since 1999, with deuterium pellets being produced as well since 2004.

The principle of operating a pellet target has been described elsewhere [1,5], and here we only briefly review those parts which are of importance for this work. Compared to the earlier work, we have undertaken more systematic studies to theoretically understand and optimize the target performance. We will describe the behavior of a pellet target on the basis of a thermodynamic analysis. We will further restrict ourselves to hydrogen pellets, but the mechanism is similar for deuterium pellets. Data values concerning hydrogen are taken from Ref. [6], as throughout this work. Concerning the micro-spheres, the naming convention used in this paper is *droplet* whenever we talk about the liquid phase and *pellet* for the solid phase, while the word *micro-sphere* covers both cases as well as the intermediate one.

2 Experimental setup

The pellet-generation system consists of four parts:

- (1) a coldhead with heat exchangers, in which pressurized hydrogen gas is cooled and liquified,
- (2) a droplet formation chamber (DFC), where a glass nozzle together with an acoustical excitation system produces and breaks-up the jet of liquid

hydrogen into uniformly spaced and sized droplets,

- (3) a vacuum injection system through which the droplets transform to totally frozen micro-spheres (and hereafter are called pellets), and
- (4) a skimmer to collimate the pellet beam.

The hydrogen is cooled by a commercially available two-stage coldhead. At stage 1, a first heat exchanger is mounted to cool the gas to about 50 K. At stage 2, a second heat exchanger regulates the temperature to 14.1 K. Inside this latter heat exchanger the gas will be liquified and brought to the nozzle directly attached at the exit, as depicted in Fig. 1. The carrier gas, helium, which is brought to the DFC in a separate channel is also cooled by this heat exchanger though it will always stay in gas phase.

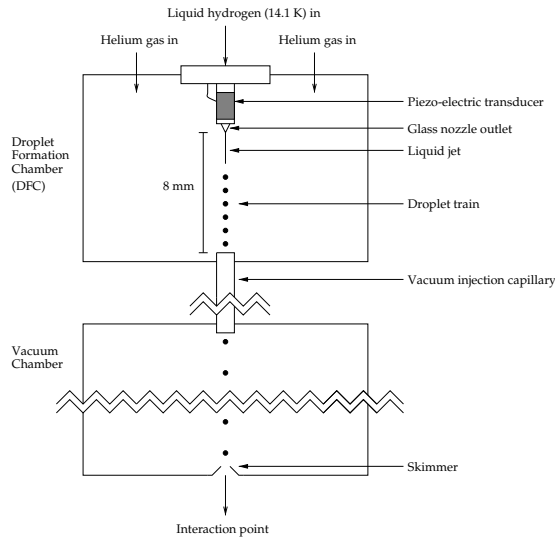


Fig. 1. A schematic picture of the droplet formation chamber and the vacuum chamber. The geometry of the DFC is complex but can be approximated by a cylinder of diameter 22 mm and height 15 mm. The distance between the nozzle outlet and the inlet of the vacuum injection capillary is 8 mm. The distance between the outlet of the vacuum injection capillary and the skimmer is 70 cm.

The breakup of the liquid hydrogen jet is a result of the acoustical excitation with axial symmetry induced by the ceramic piezo-electrical transducer connected to the nozzle (see Fig. 2). The DFC is a stainless steel chamber with four windows allowing optical observations in both transverse directions, which enables us to control the droplet formation.

The vacuum injection consists of a 70 mm long capillary, connected to a differentially pumped vacuum chamber. Another 70 cm downstream the exit of the vacuum injection capillary, a collimating skimmer is placed to skim off the pellets with too large angular divergence. The collimated pellets will proceed an additional 1.41 m before they reach the interaction point with the ion beam. As a last step they are captured by active charcoal inside the cryogenic beam dump. The mechanical details of this facility can be found in Ref. [1].

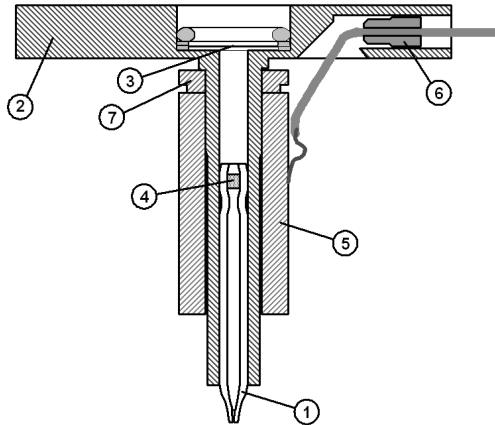


Fig. 2. A sectional drawing of the nozzle unit; showing 1) the glass nozzle, 2) the copper holder, 3) the Millipore filter ($0.5\text{ }\mu\text{m}$), 4) the stainless steel filter ($2.0\text{ }\mu\text{m}$), 5) the piezo-electric transducer, 6) the electric feed through to this, and 7) the kovar washer.

3 Operating conditions and measurements

The operating conditions of the pellet target have been developed steadily over the years. The inner diameter of the nozzle exit has decreased from initially roughly $17\text{ }\mu\text{m}$ to presently $12\text{ }\mu\text{m}$, which in turn has resulted in a pellet diameter decrease from $50\text{ }\mu\text{m}$ to a value of about $30\text{ }\mu\text{m}$. The rate of hydrogen pellets reaching the interaction point has increased from $3 \times 10^3\text{ s}^{-1}$ to almost 10^4 s^{-1} . The optimal working frequency of the transducer is conditionally determined and may vary over a wide range, typically from 60 kHz to 100 kHz. Nevertheless, for an individual experimental run the working frequency can only change within a quite narrow frequency window. It can only be determined experimentally by the observations of a “nice” droplet train, a good micro-sphere survival ratio through the vacuum injection capillary, and a strong concentration of pellets at the center of the skimmer. In this article, the logged data from the last hydrogen run in December 2003 were used as example. The conditions for this run were: a measured distance of 0.368 mm between two successive droplets in the droplet formation chamber, a transducer frequency of 102.32 kHz, a nozzle diameter $12.0\text{ }\mu\text{m}$, a pressure in the droplet formation chamber of 21.3 mbar, and a driving pressure of 729 mbar for the injected hydrogen gas.

Normally, either cooled hydrogen gas or helium gas at a temperature of about 17 K could be used as the background gas inside the DFC. To get a good pellet concentration at the skimmer one wants to have as low pressure as possible in the DFC, otherwise the angular pellet divergence from the vacuum

injection becomes too large. If the absolute pressure in the droplet chamber is too low there is a risk that the liquid jet will degenerate into a spray which immediately freezes and blocks the jet. This risk has been significantly reduced by the use of helium as background gas. The higher viscosity of helium gives a more steady gas flow through the vacuum injection capillary. As a result of this it is possible to have a higher absolute pressure in the DFC and still get a good concentration at the skimmer. The lower critical temperature of helium also eliminates the risk that the gas will liquefy in the second heat exchanger.

The ambient gas in the DFC is thus a mixture of two kinds of gases; helium and the evaporated hydrogen gas. The flow of helium is regulated by the total DFC pressure. In addition, it was found that when the helium supply was shut off, the background gas which only consisted of hydrogen had an equilibrium pressure of 8 mbar. Thus we assume that in the gas mixture the hydrogen vapor was also occupying a partial pressure of 8 mbar, and the residue 13 mbar is ascribed to helium gas for a constant total pressure of ~ 21 mbar in the DFC.

It has been theoretically and experimentally proven that the hydrogen droplets are fragile because of their rather low surface tension and thus are easily destroyed by the high-speed gas flow in the vacuum injection capillary while solid hydrogen-spheres would probably survive the vacuum injection better [7,8]. To avoid freezing of the liquid jet itself but at the same time enable the droplets to freeze as soon as possible, the temperature of liquid hydrogen at the exit of the nozzle is precisely controlled to be a slightly higher than the normal freezing temperature, $T_m = 13.96$ K, namely 14.1 K, while the total pressure, thus also the partial pressure of hydrogen vapor, in the droplet formation chamber is set to a value much lower than the triple-point pressure of hydrogen ($P_{tp} = 72$ mbar).

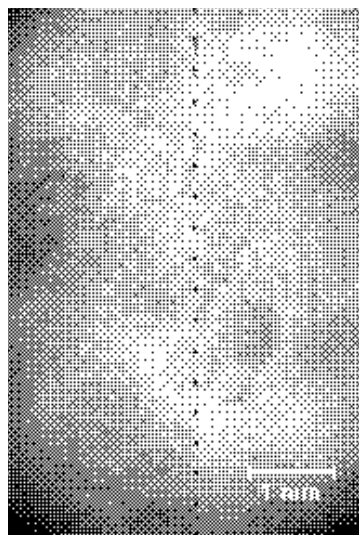


Fig. 3. A close-up of the droplet train in the droplet formation chamber showing both satellites and main droplets.

Pictures (see Fig. 3) of the droplets have been taken in the experiments by a digital camera with the assistance of a stroboscopic flash diode. The measured inter-droplet distance λ was 0.368 mm which consequently resulted in a droplet diameter of $D_d = 39.1 \mu\text{m}$ from Eq. (3). This is also consistent with the measured value of the ratio $\lambda/D_d \simeq 9$, when the droplets are just detached from the jet.

The droplet velocity v_d is deduced from $v_d = \lambda f$, where f is the driving frequency of the transducer. For our case we find $v_d = 37.7 \text{ m/s}$. The observed relative velocity decrease for droplets is measured to be about 6%, comparing droplets just detached from the jet to those close to the inlet of the vacuum injection capillary.

From experimental observations we know that the micro-spheres are in liquid phase at the inlet of the vacuum injection capillary and completely frozen at the skimmer. The latter conclusion comes from observing the micro-spheres that do not pass to really rebound like billiard balls, i.e. solid objects, as indicated in Fig. 4. The first conclusion arises from tilting the droplet train to hit the capillary inlet. In this case we do not observe the “egg shells” as described in Ref. [9] which should have been the result if the micro-spheres been partially frozen. To conclude our observations, the micro-spheres must freeze somewhere in between the inlet of the vacuum injection capillary and the skimmer.

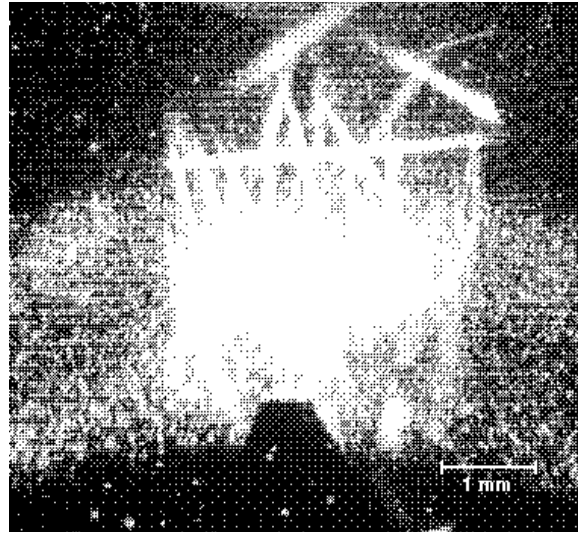


Fig. 4. Shown is the pellet concentration lit by a laser just above the skimmer, visible as the black cone in the lower part. Its opening diameter is 0.59 mm. We also see the traces of pellets bouncing around, confirming that they really are solid at this location, i.e. 70 cm downstream of the outlet of the vacuum injection capillary. The horizontal pattern comes from the monitor which the photo is taken of. This also makes the pellet concentration to look significantly bigger compared to the original frames from the CCD camera.

The calculations (see Fig. 6) show that the hydrogen droplets are cooled down so fast by evaporative cooling that a solid micro-sphere (pellet) or at least a solid shell at the droplet surface could be formed at the exit of the droplet formation chamber (inlet of vacuum injection capillary). Clearly a phenomenon called supercooling is inevitably encountered, as has been mentioned before but not examined in greater detail [1]. It is still not clear how much of the pellet beam divergence is ascribed to the supercooling, but as mentioned the pellet survival rate may be deeply affected by this phenomenon.

The gas flow in the vacuum injection capillary will be “choked” due to the large pressure difference in the DFC and the vacuum chamber. The droplet carried by the gas flow will endure a drag force given by Eq. (5) and as a result the droplet will be accelerated. We have experimentally measured the average pellet velocity of hydrogen from the pictures of the pellets just after the vacuum injection capillary. For this particular run, the average over 52 distances together with the transducer frequency resulted in a pellet velocity of 94 m/s. For other runs, the typical values range from 60 m/s to 100 m/s dependent on the pressure in the DFC and the driving pressure of hydrogen gas to the nozzle. At the moment the distribution of the pellet velocity is unknown, but we will report on these experiments in a forthcoming paper.

A crucial topic originating from the vacuum injection is the pellet beam divergence which causes about 80 percent of the produced hydrogen pellets to be skimmed off because of their too large angular spread, i.e. most of them never reach the interaction point. The origin of this type of divergence is not known in detail [10].

Pellet beam profiles measurements were carried out by step-wise moving the pellet beam over the skimmer aperture while counting the ones that pass. The results are shown in Fig. 5. *A priori* the shape of the uncollimated beam, i.e. before the skimmer, is unknown. However, by fitting several test-functions to the experimental results a Gaussian shape reproduces the measured values the best. Since the size of the pellet beam is similar to the skimmer diameter, the convolution between the two becomes important. We assumed the uncollimated beam to be a symmetric Gaussian, and by fitting its convoluted result to the experimental measurements the “real” pellet beam profile, with a FWHM of 1.04 mm, was obtained.

From comparing the total number of pellets in the uncollimated beam to the transducer frequency, a survival ratio of 50% was deduced. This rather low number is also supported from the photos taken just below the vacuum injection capillary. They indeed show that the inter-pellet distance is sometimes twice the distance of others. Thus a pellet in such a case is “missing”.

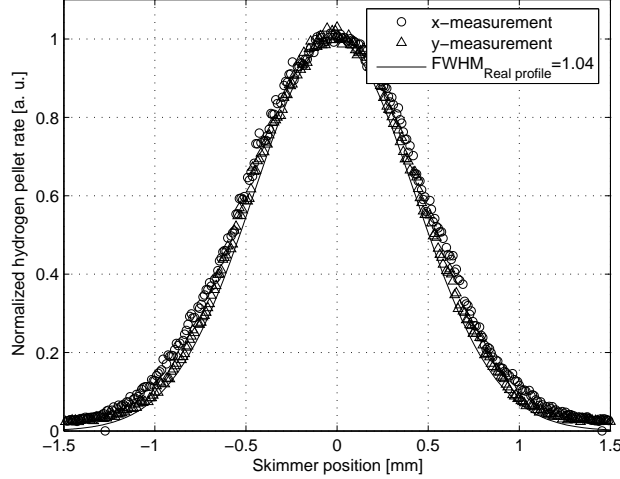


Fig. 5. Measured hydrogen pellet beam profile at the skimmer, i.e. 70 cm from the vacuum injection capillary exit. The scans are carried out in both directions. The skimmer diameter was 0.59 mm and the corrected symmetric Gaussian for the real beam had a FWHM of 1.04 mm.

4 Interpretation of the results

4.1 Droplet formation

It is well known that pressurized liquid ejected from a nozzle will form a jet. A cylinder of jet is dynamically unstable under the action of surface tension. When a vibration of a certain frequency is applied to the nozzle the corresponding wavelength λ will force the jet to disintegrate into a stream of uniform-sized droplets. From Lord Rayleigh's analysis the disturbance to the shape of the droplets grows most rapidly at an approximate wavelength of $\lambda = 4.5D_{\text{jet}}$, where D_{jet} is the diameter of the jet [11,12]. In our case the working frequency has to be set at a much lower frequency than this optimal one to avoid the coalescence effect causing clustering in the high-frequency mode. We have observed experimentally, like others [13] also have, that satellite droplets are inevitably formed accompanying the main droplets, quite independent of the experimental configuration. However, we can tune the transducer frequency slightly so that the satellite droplets could merge into the main droplets as quickly as possible due to their different velocities. For details of the nozzle unit, see Fig. 2.

4.1.1 Droplet size determination

To determine the droplet size one needs to know the jet diameter. However, the small jet size for a 12- μm nozzle in a cryogenic environment is difficult to

be measured directly. We apply fluid dynamics to overcome this problem.

In fluid dynamics the Reynolds number, defined as $\text{Re} = \rho v_{\text{noz}} D_{\text{noz}} / \mu$, is used to distinguish between different types of flows. Here, ρ is the density of liquid hydrogen, v is the fluid velocity, and μ is the dynamic viscosity. When $\text{Re} \lesssim 2000$ the flow is always laminar, and when $\text{Re} > 4000$ it is always turbulent [10]. For a $12.0 \mu\text{m}$ inner-diameter nozzle we get $\text{Re} \simeq 36v$ for hydrogen, which means that in order to have a laminar flow the hydrogen fluid must have a velocity $\lesssim 55 \text{ m/s}$. This is indeed the case, because of the discussion in Sec. 4.1.2, resulting in a Reynolds number of about 1000.

Most of the pressure drop between the driving pressure and the much lower pressure in the droplet formation chamber will take place near the exit of the nozzle, where the narrowing of the pipe system becomes significant.

Using the equations of continuity and momentum conservation, we can easily find that for laminar flow the mean velocity of the liquid fluid inside the nozzle (\bar{v}_{noz}) and the velocity of jet (v_{jet}) are related as [14]

$$v_{\text{jet}} = \frac{4}{3} \bar{v}_{\text{noz}}. \quad (1)$$

The corresponding relationship between the diameter of the fluid inside the nozzle and the diameter of the jet is given by

$$D_{\text{jet}} = \frac{\sqrt{3}}{2} D_{\text{noz}} \approx 0.866 D_{\text{noz}}. \quad (2)$$

To summarize: for the present nozzle with a $12\text{-}\mu\text{m}$ inner diameter we expect a laminar flow inside the nozzle and the jet size to be $10.4 \mu\text{m}$.

It has been further derived that in turbulent flow case the ratio between the diameter of the jet and inner diameter of nozzle ($D_{\text{jet}}/D_{\text{noz}}$) will be less than 0.866 if we solve the momentum-conservation equation with the velocity distribution of turbulent flow. This could explain why the experimental measured values of this ratio by other authors are somewhat smaller (e.g. a value of approximately 0.80 was given by Ref. [15]).

The unstable jet will break up into droplets due to the acoustic excitation. After the satellite droplets merge into the main droplet, the volume conservation gives [15]

$$D_{\text{d}} = \sqrt[3]{\frac{3}{2} D_{\text{jet}}^2 \lambda}, \quad (3)$$

where D_{d} is the droplet diameter, and λ is the wavelength jet turbulence, equivalent to the distance between the neighboring droplets. From our measured $\lambda = 0.368 \text{ mm}$ we got $D_{\text{d}} = 39.1 \mu\text{m}$.

4.1.2 Droplet velocity evolution

When the droplet is detached from the jet, an extra force will be exerted by the surface tension, σ , which pulls the fluid back towards the nozzle. This excess pressure integrated over the cross section of the jet is $-P = -2\sigma/D_{\text{jet}}$. The momentum conservation gives [16]

$$v_d \approx v_{\text{jet}} - \frac{2\sigma}{\rho D_{\text{jet}} v_{\text{jet}}}, \quad (4)$$

where v_d is the droplet velocity, and σ is the surface tension of hydrogen liquid.

Now that the droplet velocity was 37.7 m/s, we can trace back to the jet velocity and obtain $v_{\text{jet}} = 37.9$ m/s. Recalling the relationship between the jet velocity and the fluid velocity inside the nozzle, Eq. (1), numerically, the fluid velocity at the exit of the nozzle was 28.4 m/s, thus less than 55 m/s to fulfil the requirements of laminar flow (see Sec. 4.1.1).

When the droplet travels in the surrounding of gas mixture, the gas actually acts as a viscous fluid and exert a frictional drag force on it. For an isolated spherical droplet, based on Newton's resistance law, the general expression for the drag force in a gas surrounding can be written as [17]

$$F_D = -C_D \frac{\pi}{8} \rho_g D_d^2 v_{\text{rel}}^2 / C_c \quad (5)$$

Here C_D is the drag factor, which has different forms for different regions of the Reynolds number of the droplet, $\text{Re}_d = \rho_g v_{\text{rel}} D_d / \mu_g$. Further, ρ_g is the gas density, μ_g is the gas viscosity, C_c is Cunningham non-continuum correction (which is almost 1.0 in our case because we are working in the continuum region, see Sec. 4.1.3.1), A_d is the cross sectional area of the droplet, i.e. $A_d = \pi D_d^2 / 4$, and v_{rel} is the relative velocity between the droplet and the surrounding gas. Since the gas in the droplet formation chamber can only be pumped away via a 0.8 mm narrow vacuum injection capillary, this limits gas flow such that the resulted bulk gas velocity in the droplet formation chamber is insignificantly small. Therefore the background gas in the DFC could be assumed as stagnant and the relative velocity v_{rel} to equal the droplet velocity v_d . It should be kept in mind that the surrounding gas is actually a mixture of hydrogen vapor and helium gas, and the density is the linear combination of specific volumes, while the viscosity is deduced according to the summing rule of Wilke [18].

For a hydrogen droplet with a velocity of 37.7 m/s, the Reynolds number is $\text{Re}_d=34.4$. Relevant values for the background H₂-He gas at 17 K were calculated to $\rho_g = 0.049 \text{ kg/m}^3$ and $\mu_g = 2.1 \times 10^{-6} \text{ Pa s}$. The hydrogen data for this calculation were taken from Ref. [6]. The drag factor equation suitable

for a Reynolds number region of $2 < \text{Re}_d < 500$ is described as [17]

$$C_D = \frac{24}{\text{Re}_d} [1 + 0.15\text{Re}_d^{0.687}]. \quad (6)$$

This will result in a drag force of about 3000 higher than the gravitational force exerted on a droplet. Thus the gravity can be omitted and the dynamic equation for the droplet can then be written as [17]

$$\frac{dv_d}{dt} = -\frac{18\mu_g v_d}{\rho D_d^2} [1 + 0.15\text{Re}_d^{0.687}] \quad (7)$$

When the droplet passes through the DFC its diameter changes very little, so as a first order of estimation we can assume that the droplet diameter is constant. The numerical calculations of Eq. (7) show that the relative velocity loss $(1 - v_d/v_d^0)$ will be 16% when the droplet has travelled an available 7 mm distance inside the DFC (assuming the jet length in Fig. 1 to be 1 mm). Here v_d^0 is the initial droplet velocity (37.7 m/s). The observed relative velocity loss for droplets is only about 6% from the photos, which is just one-third of the above value for an isolated droplet. The difference may be explained by the effect of inter-droplet interactions within the droplet train, which means that a succeeding droplet in the wake of a proceeding droplet will endure less drag force [19]. Further effects of the inter-droplet interaction will be discussed in the next section.

4.1.3 Thermodynamic behavior of the droplet

The mass loss due to evaporation and the connected temperature development of the droplet can only be achieved by solving the appropriate thermodynamic equations of the droplet in the DFC. Many theoretical models exist to describe the heat and mass transfer processes from micro-droplets [20,21] to the surrounding for single isolated droplets. However, these models are of limited benefit in the case of a droplet train where the inter-droplet separation distance is so small that droplet-droplet interactions become significant. The intensity of interactions can be defined in terms of an interaction parameter which is the ratio between the rate of a transfer process from a droplet in an array compared to that from a single isolated droplet. Because the heat and mass transfer behave very similar, we can reasonably assume that the interaction parameters for heat and mass transfer rates are equal, and defined as [22]

$$\eta = \frac{\left(\frac{\partial m}{\partial t}\right)_{\text{arr}}}{\left(\frac{\partial m}{\partial t}\right)_{\text{iso}}}, \quad (8)$$

which is the ratio between the mass loss of a droplet in a linear array (train) relative to that from a single isolated droplet. The parameter η depends only

on the dimension-less spacing between the droplets which is defined as $\epsilon = \lambda/a$, where a is the droplet radius. From other experiments it has been reported that the inter-droplet interactions are significant ($\eta \sim 0.3$) for $\epsilon < 7.0$ but negligible for $\epsilon > 20$ [22,23]. In our case $\epsilon = 18.8$, so we have assumed η to be about 0.8.

4.1.3.1 Mass loss equation Once a droplet is formed, we assume it to (i) represent all other droplets; (ii) be totally spherical; (iii) enter a uniform environment with respect to pressure and temperature; and (iv) be surrounded by its own evaporating gas in a quasi-steady equilibrium state at the liquid surface so that the gas pressure follows the saturation line [6]

$$\ln P_S = 15.52059 - \frac{102.7498}{T_s} + 5.338981 \times 10^{-2} T_s - 1.105632 \times 10^{-4} T_s^2, \quad (9)$$

where P_S is given in Pa if the dimension of the surface temperature T_s is K. The heat and mass transfer process depends on the degree of rarefaction for the system, which is represented by the dimensionless Knudsen number defined as $\text{Kn} = l_{\text{mfp}}/D_d$ [24]. Here, l_{mfp} is the mean free path, i.e. the average distance between molecule collisions, and D_d is the droplet diameter. The ambient gas is a mixture of helium and hydrogen, so in the simple kinetic gas theory (with the approximation of rigid spheres) the mean free path is [25]

$$l_{\text{mfp}} = \frac{k_B T_\infty^{\text{mix}}}{\pi \sqrt{2} \left(\frac{1}{2} (d_{\text{He}} + d_{\text{H}_2}) \right)^2 P_\infty^{\text{mix}}}, \quad (10)$$

where k_B is Boltzmann's constant, and $d_{\text{He}} = 2.15 \text{ \AA}$ and $d_{\text{H}_2} = 2.71 \text{ \AA}$ are the sphere diameters of helium and hydrogen molecules, respectively [26]. It is expected that $l_{\text{mfp}} \sim 0.04 \mu\text{m}$ and $\text{Kn} \sim 0.01$. It is claimed in Ref. [24] that at the "diffusion-controlled continuum or near-continuum limit" the evaporation is best predicted by a diffusion-controlled model if the concentration of the inert gas is neither too large nor tending to zero when compared to the evaporated gas. In our case the partial pressures of helium and hydrogen are of the same order and hence a diffusion-controlled model should be adequate.

We can thus use Fick's first law of diffusion, $\mathbf{j}_\alpha = -\mathcal{D}_{\alpha\beta} \nabla \rho_\alpha$, to describe the movement of one chemical species α through a binary mixture of α and β . Here, j_α is the mass flux rate, the proportionality factor $\mathcal{D}_{\alpha\beta}$ is the diffusion coefficient, and $\nabla \rho_\alpha$ is the concentration gradient of α . For a spherically symmetric geometry this diffusion equation can be expressed as [19,21,27]

$$\frac{\partial m_\alpha}{\partial t} = -A \mathcal{D}_{\alpha\beta} \frac{\partial \rho_\alpha}{\partial r} \Big|_{r=a} \simeq -4\pi a^2 \mathcal{D}_{\alpha\beta} \left(-\frac{\rho_\infty - \rho_a}{a} \right) = -4\pi a \mathcal{D}_{\alpha\beta} (\rho_a - \rho_\infty). \quad (11)$$

where $\frac{\partial m_\alpha}{\partial t}$ is the mass change, A is the droplet surface area $A = 4\pi a^2$, a is the droplet radius ($a = D_d/2$), and ρ_a and ρ_∞ are the evaporated gas concentrations at $r = a$ and $r = \infty$, respectively.

For a droplet train moving in the ideal gas mixture, Eq. (11) can further be expressed as

$$\frac{\partial m_\alpha}{\partial t} = -\eta \frac{4\pi a \mathcal{D}_{\alpha\beta}}{R_\alpha} \left(\frac{P_a}{T_a} - \frac{P_\infty}{T_\infty} \right), \quad (12)$$

where $R_\alpha = R/M_\alpha$ is the specific gas constant for α and, in turn, α and β corresponds to hydrogen and helium, respectively. Here, the assumption of a quasi-steady equilibrium give $P_a = P_s$, given in Eq. (9). The diffusion coefficient of gas mixture $\mathcal{D}_{\alpha\beta}$ can be deduced from the kinetic theory as shown in Ref. [25]. We have also inserted the earlier discussed η -factor to take inter-droplet effects into account.

Since the droplet is non-stationary the mass transfer must be multiplied by a factor, the Sherwood number, due to the forced convection. Under the assumption of a negligible internal circulation inside the droplet, as has been experimentally investigated in a similar setup and concluded to be reasonable [28], the Sherwood number for mass transfer is given by [29]

$$Sh = 2.0 + 0.552 Re_d^{1/2} Sc^{1/3}, \quad (13)$$

where the Schmidt number, $Sc = \mu_g/\rho \mathcal{D}_{\alpha\beta}$, is estimated for the gas mixture.

4.1.3.2 Heat balance equation Inside a droplet the temperature profile is given by [19]

$$\rho C_P \frac{\partial T}{\partial t} = \frac{k}{r^2} \frac{\partial}{\partial r} \left(r^2 \frac{\partial T}{\partial r} \right), \quad (14)$$

for $0 \leq r \leq a(t)$ and where ρ , C_P , and k are the density, the heat capacity and the thermal conductivity of the droplet, respectively. T is the droplet temperature at the radial position r , at time t . Eq. (14) applies with the boundary conditions

$$\frac{\partial}{\partial r} \underbrace{T(0, t)}_{T_c(t)} = 0 \quad (15)$$

$$T(a, t) = T_s(t), \quad (16)$$

where the subscripts s and c , respectively, denote surface and center.

At the droplet surface, the heat balance equation can be written as [19]

$$4\pi a^2 k \frac{\partial T}{\partial r} \Big|_{r=a} = \dot{Q}_{\text{vap}} + \dot{Q}_{\text{conv}}, \quad (17)$$

with

$$\dot{Q}_{\text{vap}} = h_{\text{vap}} \frac{\partial m}{\partial t}, \quad (18)$$

and

$$\dot{Q}_{\text{conv}} = \eta 4\pi a^2 h_c (T_{\infty} - T_s). \quad (19)$$

Here, h_{vap} is the latent heat of vaporization and $h_c = \text{Nu}k/2a$ is the convective heat transfer coefficient. The Nusselt number Nu for convective correction can be expressed as [29]

$$\text{Nu} = 2.0 + 0.552 \text{Re}_d^{1/2} \text{Pr}^{1/3} \quad (20)$$

where the Prandtl number $\text{Pr} \simeq 0.70$ [31].

4.1.3.3 Droplet temperature results With these mass and heat transfer equations, the behavior of the hydrogen droplet can be obtained using an updated program version with the numerical iteration method as used earlier in Ref. [30]. With an initial droplet diameter of $39.1 \mu\text{m}$, a velocity of 37.7 m/s , and a temperature of 14.1 K , we see in Fig. 6 the droplet temperature evolution in the DFC for different cases. Our ambient pressure was 21.3 mbar with a partial hydrogen pressure of 8 mbar . The background gas temperature was assumed to be 17 K , however, the variation of this value was shown to be negligible. To simplify the calculation, the density change which takes place at the transition between the liquid and solid phase (about 12%), was neglected and instead an average value was used.

When no supercooling occurs, liquid hydrogen transforms to solid at $T_m = 13.96 \text{ K}$ and this happens for the surface of the droplet already after $2.5 \times 10^{-8} \text{ s}$. Assuming a smooth inward-directed freezing process, the whole micro-sphere would turn solid at 0.24 ms corresponding to a flight path of 10 mm about 3 mm into the vacuum injection capillary. This does not correspond to our experimental observations, because before a solid pellet is formed the micro-sphere should be partially frozen and thus fragments of frozen hydrogen should be visible if the nozzle and thereby the droplet train is tilted to hit the capillary inlet. Those fragments have never been observed and therefore we conclude that an additional mechanism must be present. One distinct possibility is the presence of supercooling resulting in the corresponding temperature lines in Fig. 6. To simulate supercooling for the hydrogen droplet, we have assumed that all thermodynamic parameters of liquid hydrogen can be extrapolated to the temperatures lower than the normal melting temperature. If not stated otherwise, the droplet train effect is $\eta = 0.8$ and the number of layers, to account for the radial temperature distribution from Eq. (14), is 50. We see that changing η to 1.0 (no effect) make almost no difference. More surprisingly is, maybe, the small difference between the droplet with constant temperature distribution (distillation limit model) and the finite-conductivity model as described above.

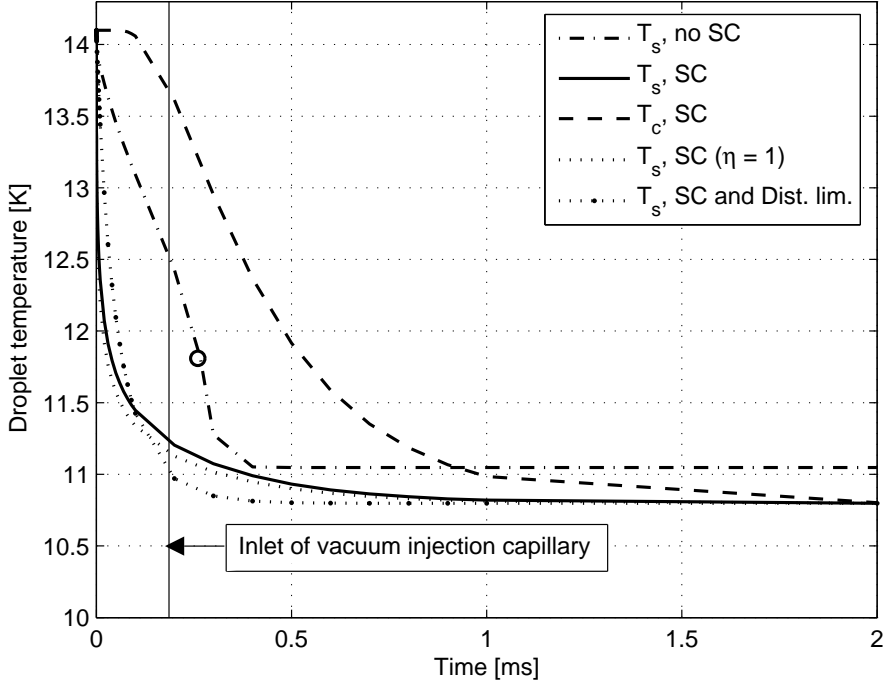


Fig. 6. Droplet temperature vs. time for initial droplets of $39.1\ \mu\text{m}$ and 14.1 K for different cases. SC is short for supercooling, whereas T_s and T_c denote surface and center temperatures, respectively. The circle marks the time where the whole pellet is solid, if no supercooling is considered. The vertical line at 0.19 ms corresponds to the available time in the droplet formation chamber.

4.1.3.4 Nucleation rate of hydrogen Generally, the reason for supercooling is that the crystallization has no place to take root and the molecular motion prevents the substance from freezing. The temperature T_n at which a droplet of volume V_d will start to freeze, is determined by the relation [38,39]

$$N_n = -V_d \int_{T_n}^{T_m} \frac{\Gamma(T)}{\dot{T}} dT \simeq 1, \quad (21)$$

where N_n is the number of nuclei and \dot{T} is the temperature change. The time dependence from the latter makes it possible to find a corresponding static formula,

$$\tau \simeq \frac{1}{\Gamma V_d}, \quad (22)$$

where τ is the lifetime of the supercooled droplet before freezing. Eq. (22) has been experimentally investigated for parahydrogen (p-H₂) and, to some extent, also normal hydrogen (n-H₂) [32,34]. They measured τ and V_d to obtain the nucleation rate Γ , in an helium environment of $\sim 15\text{ bar}$. Our case a comparable low ambient pressure, $\sim 20\text{ mbar}$, and we will therefore neglect this effect such that the theory of classical nucleation rate can be used. Furthermore, we note that the nucleation temperature of interest is not too far

away from the melting temperature, so by using the notation of Ref. [33], we get

$$\Gamma = \frac{n_L k_B T}{h} e^{-(\phi_{LS} + \delta F_0)/k_B T}, \quad (23)$$

with

$$\delta F_0 = \frac{16\pi}{3} \frac{\alpha_{LS}^3}{n_S^2 (f_L - f_S)^2}. \quad (24)$$

and

$$f_L - f_S \approx 0.99(T_m - T) - 0.029(T_m - T)^2, \quad (25)$$

for the case of parahydrogen. Here k_B is Boltzmann's constant, h is Planck's constant, n_L is the number of molecules per unit volume in the liquid phase, $\phi_{LS} = \phi_L = 45k_B$ is the activation energy for self-diffusion in the liquid, δF_0 is the maximum free energy required to form a small solid sphere in the liquid, α_{LS} is the liquid-solid surface free energy which was determined to be $0.874 \times 10^{-3} \text{ J/m}^2$ (according to the best fit of experimental data [32]), n_S is the number of molecules per unit volume in the solid phase, and f_L and f_S are, respectively, the free energies per molecule in the liquid and solid phases.

To turn back to normal hydrogen we use the results of Ref. [34] where it is pointed out that the nucleation rate for n-H₂ was measured to be $\sim 10^3$ times higher than that of p-H₂, possibly due to the “onset of rotational ordering in the solid phase”. From this and Eqs. (23), (24), and (25) the approximate nucleation rates for n-H₂ can be obtained, see Tab. 1.

T [K]	Γ [$\text{cm}^{-3}\text{s}^{-1}$]	T [K]	Γ [$\text{cm}^{-3}\text{s}^{-1}$]
9.8	4.9×10^{11}	10.8	1.7×10^0
10.0	1.3×10^{10}	11.0	2.4×10^{-4}
10.2	1.7×10^8	11.2	4.3×10^{-9}
10.4	1.1×10^6	11.4	5.0×10^{-15}
10.6	2.5×10^3	11.6	1.4×10^{-22}

Table 1

Assumed nucleation rate for hydrogen (n-H₂) at low (zero) ambient pressure, based on Eq. (23) and the experimental factor $\sim 10^3$ [34].

When nucleation occurs the latent heat of fusion is liberated, and the droplet warms up to the so-called recalescence arrest temperature T_r [34,35]. Eventually the heat stored in the droplet is exhausted, and it rapidly freezes to solid (pellet).

For a $\sim 39 \mu\text{m}$ -diameter droplet the volume is $3 \times 10^{-8} \text{ cm}^3$. According to Eq. (22) and values from Tab. 1, the needed droplet temperature is 9.8 K for the nucleation to start inside the DFC at about 0.19 ms. As seen in Fig. 6 this temperature will never be reached, not even if the DFC was extended to several decimeters. In fact, the lowest droplet temperature of 10.8 K corresponds to

a nucleation rate which is 11 orders of magnitude to low for a nucleation trigger. Given that the nucleation rate may have a large uncertainty, this huge order anyway points to that freezing in the DFC is impossible because the droplet is not “supercooled enough” to experience a phase transition to solid. Besides, if we consider the supercooling-case for the droplet center and surface temperature, respectively, i.e. the dashed and solid lines in Fig. 6, at the correspondent time for the inlet of the vacuum injection capillary, we actually have $T_c = 13.6\text{ K}$ and $T_s = 11.2\text{ K}$. That is greater than 10.8 K and thus an even lower nucleation rate.

In the calculations we have changed all related working parameters, such as the vapor pressure, the background gas pressure, and the background gas temperature. It is found that only when the pressures of vapor and background gas have been decreased to as low as 3 mbar and 10 mbar, respectively, the droplet can finally reach 9.8 K in the DFC. This will however be very hard to achieve experimentally since the hydrogen vapor pressure results from the evaporation mechanism itself and the pumping power in the DFC is limited by the narrow vacuum injection capillary.

To trigger the nucleation and thereby the freezing other means are needed. A controlled introduction of impurities might be the solution, e.g. as mentioned in Ref. [32] by heating a fine tungsten filament such that impurities at the surface are boiled off to imply a heterogenous crystallization. Or, maybe supersonic excitation can be used to decrease the degree of supercooling even further [36], and thereby increase the nucleation rate.

4.2 Pellet evaporation

Consider the possibility that the micro-spheres are still in liquid phase after they have passed the vacuum injection capillary. Using liquid parameters in the equations to come, it turns out that the droplet will reach a temperature well below 9.8 K within 0.5 ms, almost independent of chosen diameter or initial temperature. From the discussions on nucleation rate we thus conclude that if the droplet does not transform to a pellet inside the vacuum injection capillary, it will do that within some centimeters afterwards. Therefore all equations in vacuum are subscripted p for pellets.

In vacuum the pellet will evaporate in the molecular flow regime ($\text{Kn} \gg 1$), and the evaporation rate is given by the (classical) Hertz–Knudsen formula. However, a revised version also takes the bulk velocity of the vapor in vacuum into account [37], such that

$$\frac{\partial m_\alpha}{\partial t} = -1.668A \frac{P_s - P_\infty}{\sqrt{2\pi R_\alpha T}}, \quad (26)$$

where the solid-vapor saturation pressure follows [6]

$$\ln P_S = 9.2458 - \frac{92.610}{T_s} + 2.3794 \ln T_s. \quad (27)$$

The main heat source in the vacuum chamber, i.e. after the injection capillary, is the thermal radiation from the walls of the vacuum pipe. The pellets are exposed to the wall surface with a temperature of about 298 K. On the basis of the Stefan–Boltzmann law combined with Kirchhoff’s law, the thermal radiation can be written as

$$\dot{Q}_{\text{rad}} = 4\pi a^2 \varepsilon \sigma (T_w^4 - T_s^4) \quad (28)$$

where ε is the emissivity of the pellet (assumed to be 0.5), σ is the Stefan–Boltzmann constant ($5.67 \times 10^{-8} \text{ W m}^{-2} \text{ K}^{-4}$), T_w is the pipe-wall temperature (298 K), and T_s is the surface temperature of the pellet.

At the pellet surface, the energy balance gives

$$4\pi a^2 k_p \frac{\partial T_p}{\partial r} \Big|_{r=a} = \dot{m} h_{\text{sub}} + \dot{Q}_{\text{rad}} \quad (29)$$

where k_p is the thermal conductivity of the pellet and h_{sub} is the latent heat of sublimation. The energy balance equation inside the pellet is the same with that in the droplet formation chamber, i.e. Eq. (14) with the boundary conditions Eqs. (15) and (16), but for which all involved parameters should be interchanged to those of solid hydrogen.

Once the pellet is formed, we can assume that the initial temperature of the pellet will be equal to the triple point temperature 13.96 K when they are just consolidated from supercooled droplets. Of course other values are in principle possible, but due to the rapid temperature decrease the chosen temperature is really not of importance. The mass loss and temperature evolution can be calculated by solving the mass transfer and heat balance, i.e. Eqs. (14), (26), and (29). The results are shown below in Figs. 7 and 8. It turns out that pellets will cool down to about 6 K within 10 cm of travel in the vacuum chamber. As seen the lines overlap for the different cases. The relative mass loss during this process is about 14%. After that, i.e. on the way down to the skimmer and further to the interaction point, the pellet mass loss rate will be maintained at a rather low constant value. This is very important for a pellet target operation inside the vacuum of a storage ring which should not be spoiled.

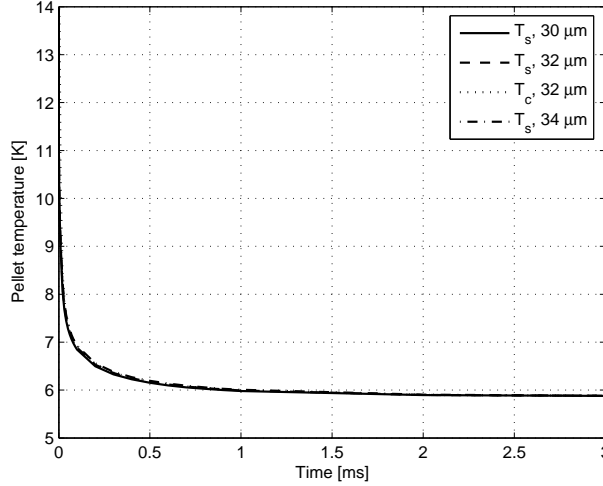


Fig. 7. The pellet temperature decreases quickly and reaches a final temperature of 5.9 K. Since there is no obvious difference between the four curves, we conclude that the temperature change is more or less independent on the initial diameter and the radial position. T_s and T_c denote surface and center temperatures, respectively.

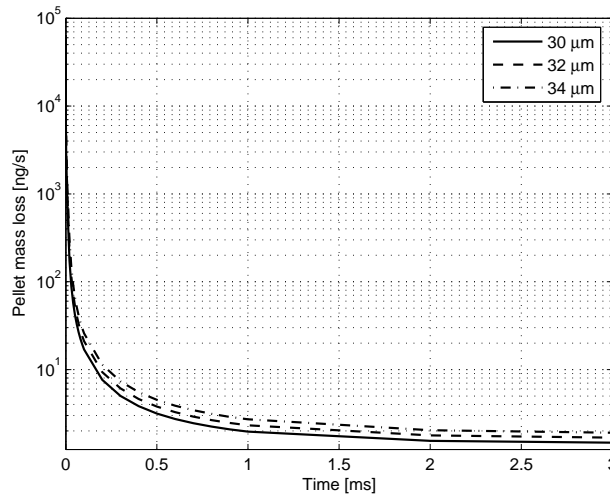


Fig. 8. The pellet mass loss becomes almost constant after about 1 ms and varies only slightly due to the initial pellet diameter. By far, most of the mass is lost during the first millisecond.

5 Summary

We have described how uniform spaced and sized droplets are formed in the droplet formation chamber by an acoustical excitation method. From experimental observations we know that the micro-spheres are in liquid phase at the inlet of the vacuum injection capillary and completely frozen at the skimmer. Thus they must freeze in between. In the absence of supercooling the calcul-

Initial diameter	$\frac{dm}{dt}(t = 0 \text{ ms})$	$\frac{dm}{dt}(t = 1 \text{ ms})$	$\frac{dm}{dt}(t = 5 \text{ ms})$
[μm]	[ng/s]	[ng/s]	[ng/s]
30	-5.7×10^4	-2.0	-1.5
32	-6.4×10^4	-2.3	-1.7
34	-7.3×10^4	-2.7	-1.9

Table 2
Mass change in vacuum for different pellet sizes and times.

lations show that they would be only partially frozen at the capillary inlet, in contradiction to the observations. However, with supercooling present the experimental observations can be explained. Our calculations show that the nucleation rate is 11 orders of magnitude too low to trigger a pellet freezing at all. It is desirable to achieve frozen pellets within the DFC, and therefore the introduction of impurities or the usage of supersonic excitation should be considered. The expected advantage of pellets formed at an earlier stage is an improvement of the survival ratio, and thus better working conditions for a pellet target.

The total relative mass loss from the formation of droplets to pellets in the reaction chamber is estimated to be 30%, corresponding to a $\sim 10\%$ decrease in diameter. The pellet size itself is actually further decreased due to the density change for hydrogen from liquid to solid. As for an original droplet with a diameter of $39 \mu\text{m}$, the final pellet size is expected to be about $33 \mu\text{m}$.

With the current setup, the droplets freeze to pellets either in the vacuum injection capillary or a few centimeters afterwards. In either case, the pellet equilibrium temperature of about 6 K is reached within 10 cm after the capillary. Our calculations show that the mass loss has converged to an almost constant value at this point. The mass loss results in an unwanted gas load. Most of the gas load will come from the mass lost during those 10 cm as well as from the skimmed off pellets eventually breaking up and evaporating in the vacuum chamber above. However, this gas load can be pumped away by appropriate vacuum pumps before and after the skimmer. Thus the gas load to consider for the vacuum system of the storage ring in which the target is installed, really originates from the converged value of the mass loss. For our pellet target this mass loss is between 1.5 and 1.9 ng/s per pellet.

Acknowledgements

We are very grateful to Curt Ekström and Inti Lehmann, whose comments considerably improved the quality of the paper. One of us (Ö.N.) acknowledges the financial support from GSI, Darmstadt, Germany, and Z.-K.L. was supported by the Chinese Academy of Sciences.

References

- [1] B. Trostell, *Nucl. Instr. and Meth. in Phys. Res. A* **362** (1995) 41.
- [2] C. Ekström, *Nucl. Instr. and Meth. in Phys. Res. A* **362** (1995) 1.
- [3] C. Ekström and the CELSIUS/WASA collaboration, *Physica Scripta T* **99** (2002) 169.
- [4] PANDA collaboration, *Letter of Intent for: PANDA*, 2004.
- [5] C. Ekström *et al.*, *Nucl. Instr. and Meth. in Phys. Res. A* **371** (1996) 572.
- [6] P. C. Souers, *Hydrogen Properties for Fusion Energy* (University of California Press, Ltd., 1986).
- [7] A. R. Hanson, E. G. Domich and H. S. Adams, *Phys. Fluids* **6** (1963) 1070.
- [8] E. Y. Harper, G. W. Grube and I.-D. Chang, *J. Fluid Mech.* **52** (1972) 565.
- [9] C. A. Foster *et al.*, *Rev. Sci. Instrum.* **48** (1977) 625.
- [10] H. O. Meyer *et al.*, *Nucl. Instr. and Meth. A* **295** (1990) 53.
- [11] Lord Rayleigh, *Proc. London Math. Soc.* **10** (1879) 4.
- [12] J.M. Schneider and C.D. Hendricks, *Rev. Sci. Instr.* **35** (1964) 1349.
- [13] W. T. Pimbley and H. C. Lee, *IBM J. Res. Dev.* **21** (1977) 21.
- [14] D. B. Harmon, Jr., *J. Franklin Institute* **259**, (1955) 519.
- [15] N. R. Lindblad and J. M. Schneider, *J. Sci. Instrum.* **42** (1965) 635.
- [16] J. Edders, *Rev. Mod. Phys.* **69** (1997) 865.
- [17] J. Yang, R. Jaenicke, V. Dreiling and T. Peter, *J. Aerosol Sci.* **31** (2000) 773.
- [18] C. R. Wilke, *J. Chem. Phys.* **18** (1950) 517.
- [19] V. Devarakonda and A. K. Ray, *Aero. Sci.* **34** (2003) 837.
- [20] R. S. Miller, K. Harstad and J. Bellan, *Int. J. of Multiphase flow* **24** (1998) 1025.

[21] H. T. Shin, Y. P. Lee and J. Jurng, *Applied Thermal Engineering* **20** (2000) 439.

[22] H. Moritz and G. Schweiger, *Chem. Eng. Technol.* **23**(2000) 4.

[23] V. Devarakonda, PH. D. Thesis, University of Kentucky, Lexington KY, USA, 1998.

[24] J. B. Young, *Int. J. of Heat and Mass Transfer* **36** (1993) 2941.

[25] R. B. Bird, W. E. Steward and E. N. Lightfoot, *Transport Phenomena*, John Wiley & Sons Inc., USA, 2nd edition (2002).

[26] R. B. Lide et al., *Handbook of Chemistry and Physics*, CRC Press LLC, 83rd (web-) edition (2003).

[27] A. V. Kozyrev and A. G. Sitnikov, *Physics–Uspekhi* **44** (2001) 725.

[28] D. R. Worsnop, Q. Shi, J. T. Jayne et al., *Aero. Sci.* **32** (2001) 877.

[29] M. Renksizbulut, R. Nafziger and X. Li, *Chem. Eng. Sci.* **46** (1991) 2351.

[30] B. Trostell, *Proc. 1st Europ. Particle Accelerator Conf., Rome, 1988* In S. Tarrazi, editor, (World Scientific, Singapore, 1989) 1424.

[31] V. D. Arp, R. D. McCarty and D. G. Friend, *NIST Technical Note* **1334** (revised), USA, (1998).

[32] G. M. Seidel et al. , *Phys. Rev. Lett.* **56** (1986) 2380.

[33] H. J. Maris, G. M. Seidel, and T. E. Huber, *J. of Low Temp. Phys.* **51** (1983) 471.

[34] H. J. Maris, G. M. Seidel, and F. I. B. Williams, *Phys. Rev. B* **36** (1987) 6799.

[35] P. Mathur, D. Apelian and A. Lawley, *Acta Metallurgica* **37** (1989) 429.

[36] T. Inada, X. Zhang, A. Yabe and Y. Kozawa, *Int. J. of Heat and Mass Transfer* **44** (2001) 4523.

[37] T. Ytrehus and S. Østmo, *Int. J. Multiphase Flow* **22** (1996) 133.

[38] J. P. Hirth, *Metall. Transactions A* **9** (1978) 401.

[39] D. Bergmann et al., *Int. J. Therm. Sci.* **39** (2000) 53.